The mass of the dark matter particle: Theory and galaxy observations

The mass of the dark matter particle: theory and galaxy observations

H. J. de Vega[a,c,1], P. Salucci[b], N. G. Sanchez[c]

[a]*LPTHE, Université Pierre et Marie Curie (Paris VI) et Denis Diderot (Paris VII), Laboratoire Associé au CNRS UMR 7589, Tour 13-14, 4ème. et 5ème. étage, Boîte 126, 4, Place Jussieu, 75252 Paris, Cedex 05, France*

[b]*SISSA/ISAS, via Beirut 4, I-34014, Trieste, Italia*

[c]*Observatoire de Paris, LERMA, Laboratoire Associé au CNRS UMR 8112, 61, Avenue de l'Observatoire, 75014 Paris, France*

Abstract

In order to determine as best as possible the nature of the dark matter (DM) particle (mass and decoupling temperature) we compute analytically the DM galaxy properties as the halo density profile, halo radius and surface density and compare them to their observed values. We match the theoretically computed surface density to its observed value in order to obtain: (i) the decreasing of the phase-space density since equilibration till today (ii) the mass of the dark matter particle and the decoupling temperature T_d (iii) the kind of the halo density profile (core or cusp). The dark matter particle mass turns to be between 1 and 2 keV and the decoupling temperature T_d turns to be above 100 GeV. keV dark matter particles necessarily produce cored density profiles while wimps ($m \sim 100$ GeV, $T_d \sim 5$ GeV) inevitably produce cusped profiles at scales about 0.003 pc. We compute in addition the halo radius r_0, the halo central density ρ_0 and the halo particle r. m. s. velocity $\overline{v^2}^{1/2}_{halo}$ they all reproduce the observed values within one order of magnitude. These results are independent of the particle physics model and vary very little with the statistics of the dark matter particle. The framework presented here applies to any kind of DM particles: when applied to typical CDM GeV wimps, our results are in agreement with CDM simulations. keV scale DM particles reproduce all observed galaxy magnitudes within one order of magnitude while GeV DM mass particles disagree with observations in up to eleven orders of magnitude.

Keywords: cosmology: dark matter, galaxies: halos, galaxies: kinematics and dynamics

1. Introduction

Since several years and more recently [37, 15, 19, 44] it has been stressed that basic galaxy parameters as mass, size, baryon-fraction, central density, are not independent from each other but in fact all of them do depend on one parameter that works as a galaxy identifier. In fact there exist functional relations that constrain the different galaxy parameters in such a way that the galaxy structure depends essentially on one parameter ([21, 38] and references therein).

These functional relations may play for galaxies the rôle that the equations of state play in thermodynamical systems.

First, let us remind that the density of DM in galaxies is usually well reproduced by dark halos with a cored distribution **(author?)** [9, 39], where r_0 is the core radius, ρ_0 is the central density $\lim_{r\to 0} \rho(r) = \rho_0$ and $\rho(r)$ for $r < r_0$ is approximately constant. Recent findings highlight the quantity $\mu_0 \equiv r_0\ \rho_0$ proportional to the halo central surface density defined as

$$2\int_0^\infty \rho(0,0,x_3)\, dx_3 \quad \text{where} \quad \vec{r} = (x_1, x_2, x_3)$$

where x_3 goes along the line of sight. The quantity μ_0 is found nearly **constant** and independent of luminosity in different galactic systems (spirals, dwarf irregular and spheroidals, elliptics) spanning over 14 magnitudes in luminosity and over different Hubble types. More precisely, all galaxies seem to have the same value for μ_0, namely $\mu_0 \simeq 120\ M_\odot/\mathrm{pc}^2$ [32, 17, 41]. It is remarkable that at the same time other important structural quantities as r_0, ρ_0, the baryon-fraction and the galaxy mass vary orders of magnitude from one galaxy to another.

The constancy of μ_0 is unlikely to be a coincidence and probably has a deep physical meaning in the process of galaxy formation. It must be stressed that μ_0 is the only dimensionful quantity which is constant among galaxies.

By analogy with the theory of phase transitions in statistical physics we find useful to call 'universal' those quantities which take the same value for a large set of galaxies while non-universal quantities vary orders of magnitude from one galaxy to another. In this context the quantities called universal take the same value up to ±20% for different galaxies.

Other known universal quantity in the above sense is the shape of the density profile when expressed as a function of r/r_0 and normalized to unit at $r = 0$.

In order to understand the above observations, we compute here from the Boltzmann-Vlasov equation [16, 30] the DM density profile and the surface density μ_0 for different types of DM.

In this paper, we follow the evolution of the gravitational collapse of a perturbation of mass $M \sim 3 \times 10^{12} M_\odot$ and derive the resulting linear halo density profile. This reproduces the phase of fast accretion found in N-body simulations. As a result, we obtain robust predictions for the properties of DM halos.

[1]Corresponding author

In the case of ΛCDM our results agree with the N-body ΛCDM simulations and in the case of ΛWDM our results agree with the observations.

We obtain a very good fit of the computed profile to the Burkert profile. This determines the relation between r_0 and the free-streaming length.

We also compute non-universal galaxy quantities as the halo radius, galaxy mass, halo central density and squared halo velocity. We find that the linear approximation provides halo central densities smaller than or in the range of the observations, and halo velocities larger than the observed ones by a factor between 1 and 10. We thoroughly analyze in our paper the validity of the linear approximation to study galaxy properties and its limitations. Notice that our determination of the DM particle mass does not relay to these non-universal galaxy quantities.

We combine the observed properties of galaxies as the effective core density and the core radius with the theoretical evolution of density fluctuations computed from first principles.

We consider in this paper the whole range of galaxy virial masses going from 5 to 300 $\times 10^{11}\ M_\odot$.

The theoretical treatment presented here captures many essential features of dark matter, allowing to determine its nature.

Our treatment also applies to CDM: if we use the CDM surface density value obtained from CDM simulations [27], we determine [sec. 9] a dark matter particle mass in the wimps mass scale (GeV), fully consistent with CDM simulations.

This paper is organized as follows: Sec. 2 presents galaxy data and empirical formulas relating basic galaxy parameters; sec. 3 deals with the phase-space density; sec. 4 contains our theoretical results for the density profile from the linearized Boltzmann-Vlasov equation. In sec. 5 we derive the DM particle mass and the decoupling temperature from the theoretical and observed galaxy surface density, in sec. 6 we compute non-universal galaxy properties and in sec. 7 we derive the profiles for keV scale DM particles and for wimps (cored vs. cusped profiles). In sec. 8 we present our conclusions.

2. DM halos around galaxies: the observational framework

The kinematics of about several thousands disk galaxies, described by the Universal Rotation Curves of Spirals, and the information obtained from other tracers of the gravitational field of galaxies, including the dispersion velocities of spheroidals and the weak lensing measurements ([21, 38] and references therein) found that the density of the dark matter halos around galaxies of different kinds, different luminosity and Hubble types is well represented, out to the galaxy virial radius, by a Burkert profile

$$\rho(r) = \rho_0\ F_B\left(\frac{r}{r_0}\right)\ ,\ F_B(x) = \frac{1}{(1+x)\ (1+x^2)}\ ,\ x \equiv \frac{r}{r_0}\ , \quad (1)$$

where ρ_0 stands for the effective core density and r_0 for the core radius. The Burkert profile satisfactorily fits the astronomical observations and we use the observed values of ρ_0 vs. r_0 for DM dominated spiral galaxies given in [38].

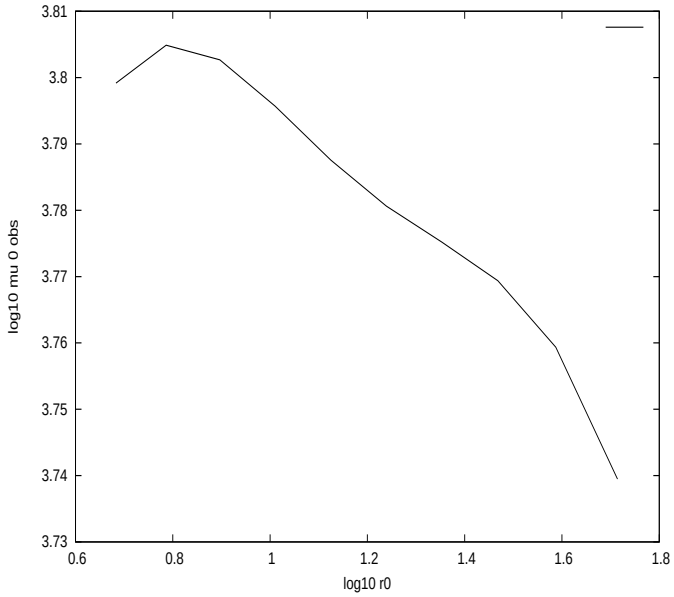

Figure 1: The common logarithm of the observed surface density $\mu_{0\,obs}$ in $(\mathrm{MeV})^3/(\hbar^2\ c^4)$ vs. the common logarithm of the core radius r_0 in kpc. Notice that in galaxies both r_0 and ρ_0 vary by a factor of thousand while μ_0 varies only by about ±20%.

The structural halo parameters ρ_0 and r_0 are found to be related, it is worth to compute from them the virial mass M_{vir} in terms of the core radius r_0 ([21, 38] and references therein)

$$m_{\rm v} \equiv \frac{M_{vir}}{10^{11} M_\odot} = 0.320\ \left(\frac{r_0}{\rm kpc}\right)^{1.72} \quad (2)$$

The surface density μ_0 is defined as:

$$\mu_0 \equiv \rho_0\ r_0 \quad (3)$$

We display in Table 1 the values of the observed surface density $\mu_{0\,obs}$ in $(\mathrm{MeV})^3/(\hbar^2\ c^4)$ and the corresponding core radius r_0. We plot in fig. 1 the observed surface density $\mu_{0\,obs}$ in $(\mathrm{MeV})^3/(\hbar^2\ c^4)$ vs. the core radius r_0.

Notice that in galaxies both r_0 and ρ_0 vary by a factor 10^3 while μ_0 varies only by less than ±20%. 5 kpc $\lesssim r_0 \lesssim$ 50 kpc for normal spiral galaxies. Therefore, as stressed by [32, 17, 41] the surface density is a constant over a large number of galaxies of different kinds.

Notice that the surface density of ordinary matter in luminous galaxies is about a factor 4 larger than the surface density value for dark matter [20]. Clusters of galaxies, exhibit a dark matter surface density about a factor 4 or 5 times larger than that of dwarf, elliptical and spiral galaxies [3, 18]. Such difference could be due to a baryons effect, which study is beyond the scope of this paper. For clusters of galaxies r_0 is 4 to 50 times larger than for the galaxies in Table 1 and the masses are 100 to 4000 larger than the masses of the galaxies in Table 1. Namely, the variation of μ_0 from galaxies to clusters of galaxies is a much small factor than the change in r_0 and in the total

r_0 (kpc)	$\mu_{0\,obs}$ (MeV^3)
4.8	0.63 10^4
6.1	0.64 10^4
7.9	0.63 10^4
10.2	0.62 10^4
13.3	0.61 10^4
17.3	0.60 10^4
22.6	0.60 10^4
29.4	0.59 10^4
38.7	0.57 10^4
51.8	0.55 10^4

Table 1: The observed core radius r_0 and the observed surface density $\mu_{0\,obs}$.

mass. We choose for the present work the data from galaxies in Table 1 (further discussion on clusters of galaxies is given in sec. 6).

3. The invariant phase-space density of DM galaxy halos

The invariant phase-space density is defined by [5, 8, 12, 28]

$$Q \equiv \frac{\rho}{\sigma^3} \qquad \text{where} \qquad \sigma^2 \equiv \frac{1}{3} \; < v^2 > \tag{4}$$

is the velocity dispersion. Q is invariant under the expansion of the universe and decreases due to self-gravity interactions [43] from its primordial value Q_p to the volume average value Q_{halo} of the galaxies today:

$$Q_{halo} = \frac{1}{Z} \; Q_p \; , \tag{5}$$

where

$$Q_{halo} \equiv \frac{\rho_{halo}}{\sigma^3_{halo}} \quad , \quad Q_p \equiv \frac{\rho_{prim}}{\sigma^3_{prim}} \; . \tag{6}$$

This equation defines the factor Z [12]. Z is larger than unity and its value depends on the galaxy considered.

Let us anticipate that Q_p only depends on the properties of the DM particle and its primordial distribution function [see eq.(11) below].

The velocity $v_{halo}(r)$ follows from the virial theorem combined with the Burkert profile eq.(1) [21, 38]

$$v^2_{halo}(r) = 2\,\pi\,G\,\frac{\rho_0\; r_0^3}{r}\left[\ln(1+x) - \arctan x + \frac{1}{2}\;\ln(1+x^2)\right] , \qquad x = \frac{r}{r_0} \qquad . \tag{7}$$

Q_{halo} is obtained by averaging $\rho(r)$ and $v^2_{halo}(r)$ over the volume using the density itself $\rho(r)$ as weight function (see Appendix A). From eqs. (1), (4), (6) and (7) we obtain [see eq.(A.4)],

$$Q_{halo} = \frac{0.069}{G^{\frac{3}{2}}\;\sqrt{\rho_0}\; r_0^3} \quad \text{(Burkert)} \; . \tag{8}$$

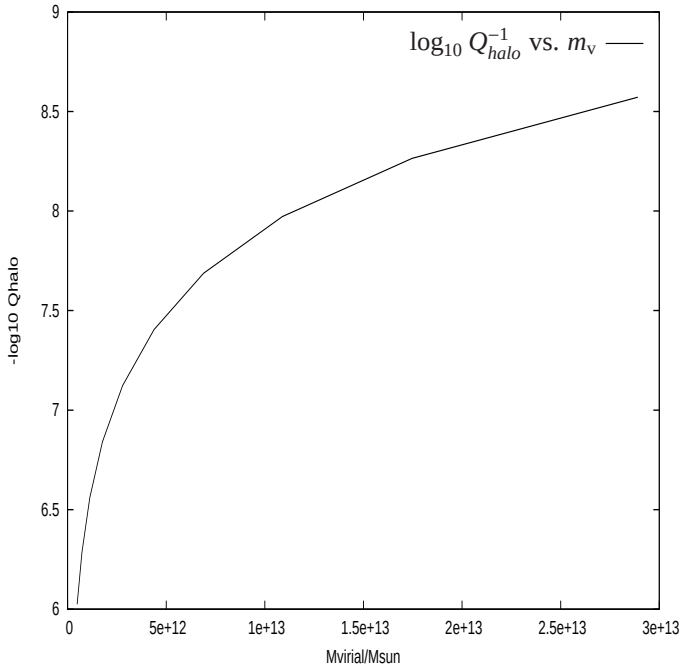

Figure 2: The logarithm$_{10}$ of the phase-space density Q_{halo} obtained from eq.(8) using the data in Table 1 vs. the virial mass of the galaxy M_{virial} in units of solar masses $M_\odot$.

For a NFW profile,

$$\rho(r) = \frac{\rho_s}{\frac{r}{r_s}\left(1+\frac{r}{r_s}\right)^2} \; , \tag{9}$$

we get:

$$Q_{halo} = \frac{0.324}{G^{\frac{3}{2}}\;\sqrt{\rho_s}\; r_s^3} \quad \text{(NFW)} \; . \tag{10}$$

Both results eqs. (8) and (10) are of the same order of magnitude and differ by a factor ~ 5. Since $Q \sim m^4$ as shown below in eq.(11), using the cuspy NFW profile instead of the cored Burkert profile only may change the DM particle mass by a factor ~ 1.5 keeping its order of magnitude.

We plot in fig. 2 the phase-space density Q_{halo} vs. the virial mass of the galaxy M_{virial} in units of solar masses $M_\odot$. Notice

that the virial mass of the galaxy is related to the halo radius r_0 through eq.(2).

The primordial invariant phase-space density Q_p can be evaluated in the radiation dominated (RD) era with the result [12]

$$Q_p = \frac{3\,\sqrt{3}}{2\,\pi^2}\,g\,\frac{I_2^{\frac{5}{2}}}{I_4^{\frac{3}{2}}}\,\frac{m^4}{\hbar^3}\,, \tag{11}$$

where I_2 and I_4 are the dimensionless momenta of the particle DM primordial distribution function [12]:

$$I_2 \equiv \int_0^\infty y^2\,F_d(y)\,dy\,,\; I_4 \equiv \int_0^\infty y^4\,F_d(y)\,dy\,,$$

g is the number of internal degrees of freedom of the DM particle ($g = 2$ for Dirac fermions). For example, for Dirac fermions of mass m that decoupled ultrarelativistically at thermal equilibrium we have,

$$Q_p = 0.020395\,\frac{m^4}{\hbar^3}\,. \tag{12}$$

Similar expressions and values are obtained for bosons and for particles decoupling ultrarelativistically out of thermal equilibrium [12].

The covariant decoupling temperature T_d can be expressed in terms of the number of ultrarelativistic degrees of freedom at decoupling g_d by using entropy conservation [4]

$$T_d = \left(\frac{2}{g_d}\right)^{\frac{1}{3}}\,T_\gamma\,. \tag{13}$$

g_d can be expressed as [12]

$$g_d = \frac{2^{\frac{1}{4}}}{3^{\frac{3}{8}}\,\pi^{\frac{3}{2}}}\,\frac{g^{\frac{3}{4}}}{\Omega_{DM}}\,\frac{T_\gamma^3}{\rho_c}\,Q_p^{\frac{1}{4}}\,(I_2\,I_4)^{\frac{3}{8}} \tag{14}$$

where T_γ is the CMB temperature today, Ω_{DM} the DM cosmological fraction and ρ_c the critical density of the universe. From WMAP/LSS data we have [34],

$$T_\gamma = 0.2348\ \text{meV}\,,\; \Omega_{DM} = 0.228\,,$$

$$\rho_c = (2.518\ \text{meV})^4/(\hbar^3\,c^5)\,, \tag{15}$$

here 1 meV $= 10^{-3}$ eV. We have in addition [12],

$$m = \pi^2\,\Omega_{DM}\,\frac{\rho_c}{T_\gamma^3}\,\frac{g_d}{g\,I_2} = 6.986\ \text{eV}\,\frac{g_d}{g\,I_2}\,, \tag{16}$$

Hence, a DM particle decoupling ultrarelativisticaly at redshift z_d and physical decoupling temperature $T_d^{phys} = (1 + z_d)\,T_d \gtrsim 100$ GeV where $g_d \sim 200$ (see ref. [30]) will have a mass in the keV scale.

4. The linear Boltzmann-Vlasov equation.

We now evolve the density fluctuations from the end of inflation till today in the standard model of the Universe. This evolution provides the phase-space density Q_{halo} and the surface density μ_0 today. The density fluctuations follow from the distribution function which evolves according to the non-linear Boltzmann-Vlasov equation. The evolution is practically linear in the RD era and in the MD era before structure formation. That is, we can use the linear Boltzmann-Vlasov for redshift $z \gtrsim 30$. For $z \lesssim 30$ non-linearities are relevant and one should use the non-linear Boltzmann-Vlasov equation or, alternatively, perform N-body simulations. It must be noticed that the resolution of the linearized Boltzmann-Vlasov equation from the end of inflation till today provides a good approximated picture of the structures today [13]. From the evolution of the dark matter fluctuations $\Delta(k, z)$ we obtained the density profile $\rho_{lin}(r)$ [13].

We follow the density fluctuations in the RD era according to the results in [16] and [29]. It is convenient to recast the linearized Boltzmann-Vlasov equation in the matter dominated (MD) era as an integral equation, the Gilbert equation [22]. We solve the Gilbert equation [13, 6] to obtain the density fluctuations $\Delta(k, z)$ till today

$$\Delta(k, z) \stackrel{z\to 0}{=} \frac{3}{5}\,T(k)\,(1 + z_{eq})\,\Delta(k, z_{eq})\,. \tag{17}$$

Here the subindex $_{eq}$ refers to equilibration, the beginning of the MD era, $1 + z_{eq} \simeq 3200$ and $T(k)$ is the transfer function which takes into account the evolution of the density fluctuations during the matter dominated era. $T(k)$ has the properties: $T(0) = 1$ and $T(k \to \infty) = 0$. Namely, the transfer function $T(k)$ suppresses the large k (small scale) modes.

It is convenient to introduce the dimensionless variable

$$\gamma \equiv k\,r_{lin} \quad \text{where} \quad r_{lin} \equiv \frac{l_{fs}}{\sqrt{3}} = \frac{\sqrt{2}}{k_{fs}}\,, \tag{18}$$

l_{fs} and k_{fs} stand for the free-streaming length and free-streaming wavenumber respectively [30] and r_{lin} is given by [6]

$$r_{lin} = 2\,\sqrt{1 + z_{eq}}\,\left(\frac{3\,M_{Pl}^2}{H_0\,\sqrt{\Omega_{DM}}\,Q_p}\right)^{\frac{1}{3}}\,, \tag{19}$$

H_0 stands for the Hubble constant today and M_{Pl} for the Planck mass,

$$H_0 = 1.5\,10^{-33}\ \text{eV}\,,\; M_{Pl} = 2.43\,10^{18}\ \text{GeV}\,. \tag{20}$$

r_{lin} is the characteristic length scale in the linear regime.

We plot in fig. 3 the transfer function $T(\gamma)$ for Fermions (FD) and Bosons (BE) decoupling ultrarelativistically, and for particles decoupling non-relativistically [Maxwell-Boltzmann statistics, (MB)]. We see from fig. 3 that the transfer function $T(\gamma)$ decreases by an amount of order one for γ increasing by unit. Therefore, $T(k)$ decreases by an amount of order one when k increases by an amount of the order of the wavenumber k_{fs} [see eq.(18)]. As we see from fig. 3, $T(\gamma)$ shows little variation with the statistics of the DM particles.

4.1. The phase density from the observed and theoretical surface density

We match in this section the observed surface density (Table 1) with the surface density computed from eqs. (29) and (30). This gives as a result eq.(36) which determines the primordial phase density.

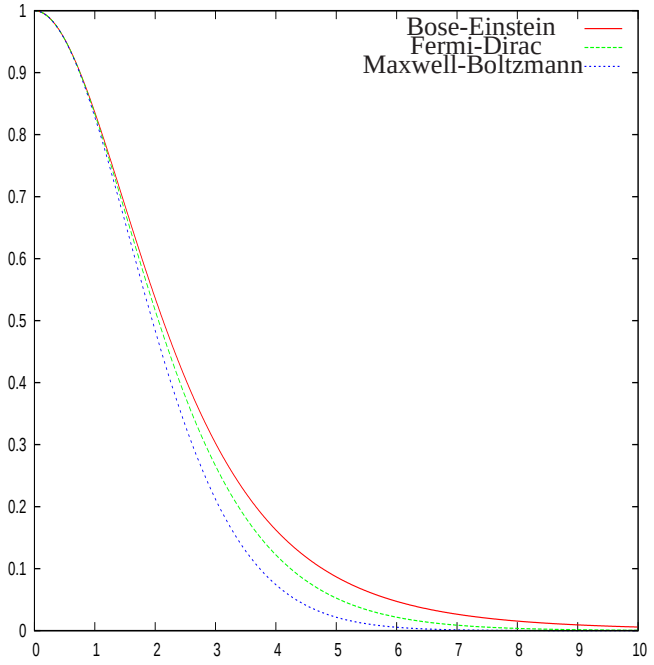

Figure 3: The transfer function $T(k)$ vs. $\gamma = k\ r_{lin}$ for Fermions and Bosons decoupling ultrarelativistically and for particles decoupling non-relativistically (Maxwell-Boltzmann statistics). $T(\gamma)$ shows little variation with the statistics of the DM particles. We see that $T(k)$ decays for increasing k with a characteristic scale $\sim 1/r_{lin} \sim k_{fs}$ which is the free-streaming wavenumber [see eq.(18)].

We first compute the linearized density profile from the Fourier transform of the density fluctuations today [13]

$$\rho_{lin}(r) = \frac{1}{2\,\pi^2\,r}\ \int_0^\infty k\ dk\ \sin(k\,r)\ \Delta(k, z=0)\ , \qquad (21)$$

More explicitly, from eq.(17) the density profile $\rho_{lin}(r)$ turns to be the Fourier transform of the density fluctuations $\Delta(k, z_{eq})$ by the end of the RD era times the transfer function $T(k)$:

$$\rho_{lin}(r) = \frac{108\ \sqrt{2}}{5\,\pi}\ \frac{\Omega_{DM}\ M_{Pl}^2}{H_0}\ (1+z_{eq})\ |\Delta_0|$$
$$\times b_0\ b_1\ \frac{k_0^{2-n_s/2}}{r_{lin}^{n_s/2}\ r}\ \int_0^\infty d\gamma\ N(\gamma)\ \sin\left(\gamma\ \frac{r}{r_{lin}}\right)\ , \qquad (22)$$

where $|\Delta_0|$ stands for the primordial power amplitude, n_s is the primordial spectral index, k_0 is the pivot wavenumber used by WMAP to fit the primordial power, k_{eq} the horizon wavenumber by equilibration and

$$N(\gamma) \equiv \gamma^{n_s/2-1}\ \ln\left(\frac{c_0\ \gamma}{k_{eq}\ r_{lin}}\right)\ T(\gamma)\ . \qquad (23)$$

The numerical values of the cosmological parameters entering in eq.(22) are [31]

$$|\Delta_0| \simeq 4.94\quad 10^{-5}\quad ,\quad n_s \simeq 0.964\quad ,\quad k_0 = 2\ \mathrm{Gpc}^{-1}\ ,$$
$$k_{eq} = 9.88\ \mathrm{Gpc}^{-1}\quad ,\quad c_0 \simeq 0.1160\ . \qquad (24)$$

All fluctuations with $k > k_{eq}$ that were inside the horizon by equilibration are relevant here [13]. This introduces in eq.(22) the comoving horizon volume by equilibration [13, 16]

$$\frac{b_1}{k_{eq}^{\frac{3}{2}}} \simeq \frac{b_1\ b_0}{H_0^{\frac{3}{2}}}\ , \qquad (25)$$

where $b_0 \simeq 3.669\ 10^{-3}$ and $b_1 \sim 1$ (actually, $b_1 = 1$ in [13]).

The initial power fluctuations are multiplied by a Gaussian random field $g(\vec{k})$ with unit variance

$$< g(\vec{k})\ g^*(\vec{k'}) >= \delta(\vec{k} - \vec{k'})\ , \qquad (26)$$

which describes the random quantum character of the primordial fluctuations.

Each realization of the random field $g(\vec{k})$ with unit variance and zero average produces a DM configuration in the linear regime (a 'galaxy'). The simplest one is obtained for $g(\vec{k}) = 1$. The presence of $g(\vec{k})$ will produce a large variety of non-spherically symmetric galaxy configurations in a large range of masses and sizes. For simplicity we restrict ourselves here to the case $g(\vec{k}) = 1$ and leave the inclusion of $g(\vec{k}) \neq 1$ to future work. The profile $\rho_{lin}(r)$ [with $g(\vec{k}) = 1$] bears the universal properties of the galaxies, that is to say, the general properties common to all (or most) galaxies. This is why such a profile is very appropriate and useful to extract these universal properties.

From the results eqs.(22)-(24) we compute and analyze the surface density and the density profile. We see from eq.(22) that $\rho_{lin}(r)$ decreases with r having r_{lin} as characteristic scale since it depends on r/r_{lin} being the Fourier transform of a function of γ that decreases with unit characteristic scale in γ [see fig. 3].

We plot in fig. B.14 the ratio

$$\frac{\rho_{lin}(r)}{\rho_{lin}(0)} \equiv \Psi(y) = \frac{\int_0^\infty N(\gamma)\ \sin(\gamma\, y)\ d\gamma}{y\ \int_0^\infty \gamma\ N(\gamma)\ d\gamma}\ \text{where}\ y \equiv \frac{r}{r_{lin}}\ , \qquad (27)$$

for Fermions (FD) and Bosons (BE) decoupling ultrarelativistically and for particles decoupling non-relativistically [Maxwell-Boltzmann statistics (MB)].

$\Psi(y)$ mainly depends on known cosmological parameters and fundamental constants and has a weak logarithmmic dependence on the DM particle mass.

We compute theoretically the surface density from the density profile eq.(22) and the halo radius eqs.(19) and (B.1). Then,

$$\mu_{0\,lin} \equiv r_0\ \rho_{lin}(0)\ , \qquad (28)$$

with eqs. (19)-(22) and (B.1), $\mu_{0\,lin}$ reads:

$$\mu_{0\,lin} = \frac{108\ \sqrt{2}}{5\,\pi}\ \Omega_{DM}\ |\Delta_0|\ (1+z_{eq})^{1-n_s/4}\ \frac{k_0^2\ M_{Pl}^2}{H_0\ \alpha}$$
$$\times b_0\ b_1\ \left(\frac{\sqrt{\Omega_{DM}}\ H_0\ Q_p}{24\ k_0^3\ M_{Pl}^2}\right)^{n_s/6}\ \int_0^\infty \gamma\ N(\gamma)\ d\gamma\ . \qquad (29)$$

The DM profile eq.(22) decreases with the characteristic length r_{lin} which is of the same order of magnitude than the halo radius r_0 in the empiric density profile eq.(1). We define

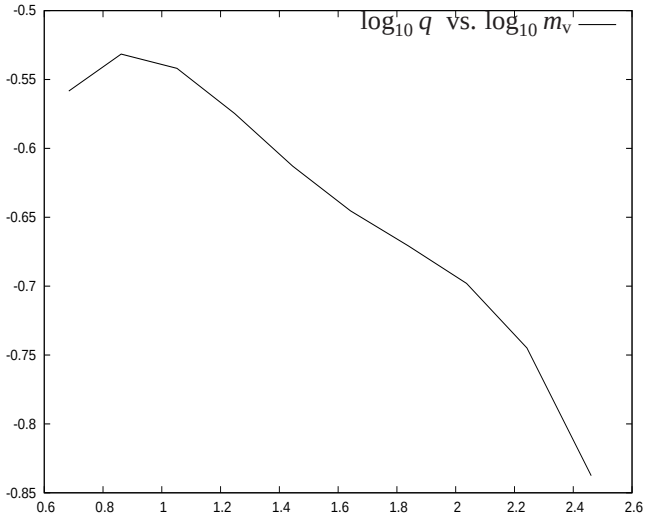

Figure 4: The logarithm$_{10}$ of the primordial phase-space density $q = (Z\ Q_{halo})/(\mathrm{keV})^4$ vs. the common logarithm of the virial mass of the galaxy $m_{\rm v} \equiv M_{virial}/[10^{11} M_\odot]$. q is obtained by solving eq.(36).

the coefficient α as $\alpha \equiv r_{lin}/r_0$ and determine it by fitting the linear profile to the Burkert profile in Appendix B. The value of α turns to be between 0.4 and 0.8 depending on the DM particle statistics (see Table B.1).

Using the numerical values of the parameters eqs. (20) and (24), this theoretical formula takes the form

$$\mu_{0\,lin} = 391.1\ \frac{(\mathrm{MeV})^3}{\hbar^2\ c^4}\ \frac{b_1}{\alpha}\ q_p^{\frac{n_s}{6}}\ \int_0^\infty \gamma\ N(\gamma)\ d\gamma\ , \qquad (30)$$

where

$$q_p \equiv \frac{Q_p}{(\mathrm{keV})^4}\ \hbar^3\ c^8 \quad , \qquad (31)$$

and

$$N(\gamma) = \gamma^{n_s/2-1}\ \ln\left(d_0\ q_p^{\frac{1}{3}}\ \gamma\right)\ T(\gamma) \quad , \quad d_0 = 556.7\ . \qquad (32)$$

From now on we use the dimensionless primordial density q_p.

We identify the observed surface density $\mu_{0\,obs}$ with the theoretical value obtained in the linear approximation $\mu_{0\,lin}$. We thus obtain the following trascendental equation in the variable q_p:

$$q_p^{\frac{n_s}{6}}\ \int_0^\infty \gamma\ N(\gamma)\ d\gamma = \frac{\alpha}{b_1}\ \frac{\mu_{0\,obs}\ \hbar^2\ c^4}{391.1\ \ (\mathrm{MeV})^3}\ . \qquad (33)$$

We compute the quantities in eq.(33) using $N(\gamma)$ eq.(31) [i. e. the transfer function $T(\gamma)$] from the solution of the linearized Boltzmann-Vlasov equation obtained in [13, 6], so that:

$$\int_0^\infty \gamma^{n_s/2}\ T(\gamma)\ \ln\gamma\ d\gamma = 1.315\ldots\ ,$$
$$\int_0^\infty \gamma^{n_s/2}\ T(\gamma)\ d\gamma = 2.666\ldots \qquad (34)$$

and hence,

$$\int_0^\infty \gamma\ N(\gamma)\ d\gamma = 18.17\left(1 + 0.0489\ \ln q_p\right)\ . \qquad (35)$$

These values correspond to fermions decoupling ultrarelativistically at thermal equilibrium. Bosons and particles obeying the Maxwell-Boltzmann statistics yield similar results as one sees from figs. 3 and B.14.

For fermions decoupling ultrarelativistically at thermal equilibrium, eq.(33) takes then the form:

$$q_p^{0.161}\ \left(1 + 0.04891\ \ln q_p\right) = \frac{1}{b_1}\ \frac{\mu_{0\,obs}\ \hbar^2\ c^4}{10330\ (\mathrm{MeV})^3}\ . \qquad (36)$$

where we used the numerical values in eqs.(24) and (35). The value of $b_1 \sim 1$ which provides the best fit to the halo radius is $b_1 \simeq 0.8$ (see appendix Appendix B).

We proceed now to solve numerically eq.(36) to obtain the primordial phase-space density q_p for the different values of $\mu_{0\,obs}$ given in Table 1.

5. The DM particle mass and the decoupling temperature from the galaxy surface density

We plot in fig. 4 the solution of eq.(36), q_p vs. $m_{\rm v}$. From eqs.(5) and (31) q_p can be expressed as

$$q_p = \frac{Z\ Q_{halo}}{(\mathrm{keV})^4}\ \hbar^3\ c^8\ . \qquad (37)$$

Therefore, for a galaxy of mass $m_{\rm v}$ the observed values of the phase-space density Q_{halo} (fig. 2) yields the factor Z as a function of the virial mass $m_{\rm v}$ [eq. (2)].

In Fig. 5 we plot $\log_{10} Z$ vs. $m_{\rm v}$, and $\log_{10} Q_{halo}^{-1}$ vs. $m_{\rm v}$ is plotted in Fig. 2. We see that Q_{halo} decreases with $m_{\rm v}$ while Z increases with $m_{\rm v}$ in such a way that the product $Z\ Q_{halo}$ is roughly **constant**. Moreover, as follows from eqs.(5) and (12) $Z\ Q_{halo}$ gives the DM particle mass

$$m^4 = 49.0\ Z\ Q_{halo}\ . \qquad (38)$$

We notice in fig. 5 that the factor Z changes by about two orders of magnitude

$$2.9\ 10^5 \lesssim Z \lesssim 5.4\ 10^7\ ,$$

over a large range of values of the virial mass. The variation of Z is relevant in the context of galaxy formation but not for the particle DM determination. Since m goes as $Z^{1/4}$ even a large change in Z merely produces a small change in m. For example, changing Z by a factor 100 changes m by a factor 3.2.

We obtain the DM particle mass m from eqs.(11)-(12) in terms of the invariant phase-space density Q_p:

$$m = m_0\ \frac{Q_p^{\frac{1}{4}}}{\mathrm{keV}} = m_0\ q_p^{\frac{1}{4}} \quad , \quad m_0 \equiv \left(\frac{2}{g}\right)^{\frac{1}{4}}\ \frac{\sqrt{\pi}}{I_2^{\frac{5}{8}}}\ \left(\frac{I_4}{3}\right)^{\frac{3}{8}}\ \mathrm{keV}\ , \qquad (39)$$

where

$$m_0 = 2.6462\ \mathrm{keV}/c^2 \quad \text{for Dirac fermions} \quad ,$$
$$m_0 = 2.6934\ \mathrm{keV}/c^2 \quad \text{for scalar Bosons.} \qquad (40)$$

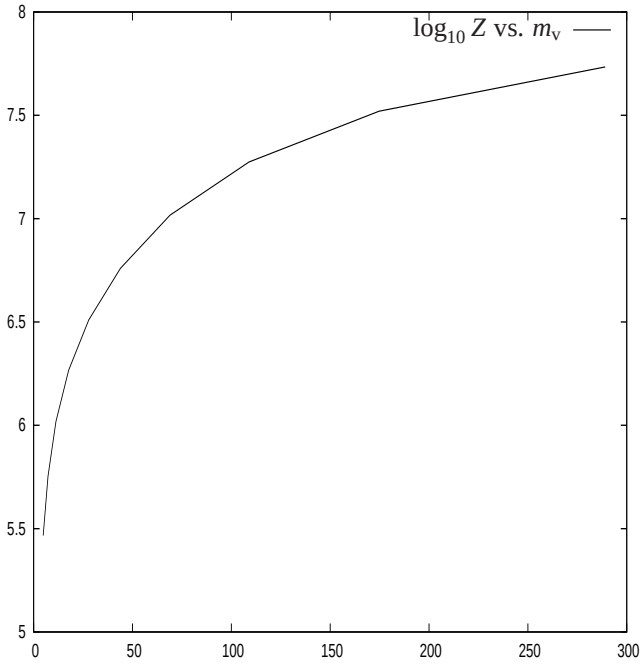

Figure 5: The common logarithm of the self-gravity decreasing factor Z computed from eq.(37) with q_p solution of eq.(36) [fig. 4] vs. the virial mass of the galaxy $m_{\rm v} \equiv M_{virial}/[10^{11} M_\odot]$.

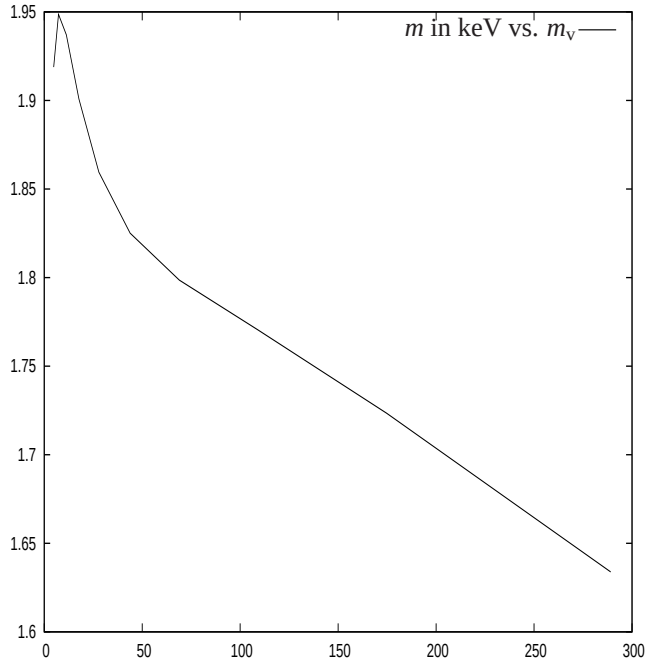

Figure 6: The DM particle mass m in keV following eq.(39) with the values of q_p solution of eq.(36) vs. the virial mass of the galaxy $m_{\rm v} \equiv M_{virial}/[10^{11} M_\odot]$. We see that the DM mass m exhibits the same variation with $m_{\rm v}$ than the surface density $\mu_{0\,obs}$ in fig. 1. The precision in the observations of the surface density μ_0 translates on the precision of the DM mass m. A value for m slightly below 2 keV is favoured.

The numerical coefficients here correspond to ultrarelativistic decoupling at thermal equilibrium. For decoupling out of thermal equilibrium the coefficients are of the same order of magnitude [12].

In fig. 6 we plot m according to eq.(39) with the values of q_p solution of eq.(36) (fig. 4) and $\mu_{0\,obs}$ given in Table 1. The precision in the observations of the surface density μ_0 translates on the precision of the DM particle mass m.

We find m about 2 keV (up to ±10%) for $b_1 = 0.8$. More generally, m is in the keV **scale** for $b_1 \sim 1$.

The variation of the observed surface density $\mu_{0\,obs}$ with the core radius r_0 (fig. 1) is similar to:

- (a) the variation of the DM particle mass m displayed in fig. 6,
- (b) the variation of the primordial phase-space density q_p in fig. 4,
- (c) the variation of the density contrast in fig. 9.

Therefore, the precision in the observations of the surface density μ_0 translates on the precision in the evaluation of the DM mass m.

From the solution for q_p eq.(36) and fig. 4 we can also compute the number of ultrarelativistic degrees of freedom at decoupling g_d and therefore the decoupling temperature T_d which is a further relevant characteristic magnitude of the DM particle. For Dirac fermions decoupling ultrarelativistically at thermal equilibrium the number of ultrarelativistic degrees of freedom at decoupling can be expressed from eq.(14) as

$$g_d = 1365.5\; q_p^{\frac{1}{4}} \; . \tag{41}$$

And from fig. 4:

$$0.14 < q_p < 0.3 \quad , \quad 0.61 < q_p^{\frac{1}{4}} < 0.74 \; . \tag{42}$$

We thus find that for thermal fermions g_d is in the interval

$$833 < g_d < 1010 \qquad \text{thermal fermions} \; ,$$

which correspond to physical decoupling temperatures [eq.(13)] above 100 GeV.

The gravitino is a popular DM candidate decoupling at thermal equilibrium which can provide such values of $g_d \sim 1000$ in non-minimal supergravity extensions of the standard model of particle physics. (In the minimal supersymmetric extension of the standard model (MSSM) one has the value $g_d = 228.75$ [23, 42]).

For DM particles decoupling out of thermal equilibrium as sterile neutrinos, the primordial power spectrum and therefore the inferred values for the mass of the DM particle change by a factor of order one [5, 7, 12, 14, 36, 46]. The low-momentum regime is enhanced in the out of equilibrium particle distributions $F_d(y)$ [5] and therefore the dimensionless momentum I_2 of

$F_d(y)$ is smaller for out of equilibrium decoupling than for thermal equilibrium decoupling. As a consequence, we see from eq.(16) that we can have smaller g_d for smaller I_2 always keeping m in the keV scale.

Sterile neutrinos which decouple out of equilibrium are today the front-runner candidate for WDM in the keV mass scale.

In summary, the DM particle mass is in the keV scale whether the DM particle decouples in or out of thermal equilibrium. The fact that the DM particle mass is in the keV scale is a robust result which does not depend on the details of the particle physics models. Of course, to fix the number within the scale $1 < m < 10$ keV depends on the details of the particle model. Our aim in this paper is not to analyze the observational constraints on the DM particle models but to determine the DM particle mass scale from general fundamental grounds and observations.

6. Non-universal structural galaxy properties

We compute here for illustration non-universal galaxy quantities as the halo radius, galaxy mass, halo central density and squared halo velocity. These calculations are independent of determination of the DM particle mass and are presented to see what kind of results provide the linear approximation. Let us anticipate that the linear approximation for non-universal galaxy properties agrees with the observed values within one order of magnitude.

Notice that our determination of the DM particle mass does not relay to these non-universal galaxy quantities.

The characteristic length of the linear profile r_{lin} eq.(19) takes the following form in terms of q_p eq.(31):

$$r_{lin} = 21.1\ q_p^{-\frac{1}{3}}\ \text{kpc}\ . \tag{43}$$

In fig. 7 we plot r_{lin} from eq.(43) and $\alpha\ r_0$ from the data in Table 1 as functions of $m_{\rm v}$.

The halo radius in the linear approximation is given by $r_{lin} = \alpha\ r_0$ which for DM Dirac fermions becomes

$$r_0 \equiv \frac{r_{lin}}{0.688} = 30.7\ q_p^{-\frac{1}{3}}\ \text{kpc}\ , \tag{44}$$

where we used $\alpha = 0.688$ obtained in appendix Appendix B by fitting the Burkert and linear profiles.

Using the range of values of q_p eq.(42) obtained by solving eq.(36) yields

$$46\ \text{kpc}\ < r_0 < 59\ \text{kpc}\ .$$

which is in the upper range of the observed r_0 values in Table 1. Namely, the linear approximation for the halo radius give values above or in the range of the observations.

The total mass of the galaxy M_{gal} follows by integrating the density profile eq.(22). We find

$$M_{gal} \simeq 20\ r_0^3\ \rho_{lin}(0) = 20\ r_0^2\ \mu_{0\,obs}\ . \tag{45}$$

In fig. 8 we plot M_{gal}/M_{virial} vs. $m_{\rm v}$ where the observed $m_{\rm v}$ and M_{virial} are defined by eq.(2).

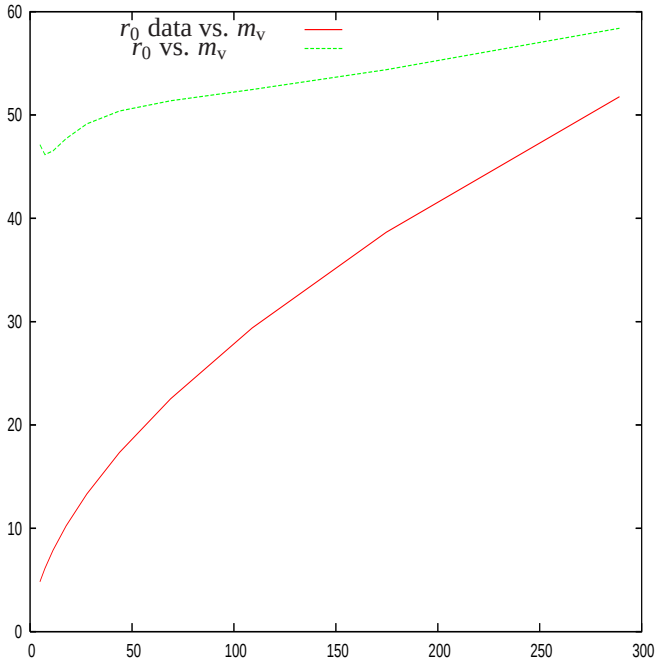

Figure 7: The computed halo radius r_0 in kpc from eq.(44)in broken green line, the halo radius r_0 in kpc from the real data in Table 1 in solid red line vs. the virial mass of the galaxy $m_{\rm v} \equiv M_{virial}/[10^{11} M_\odot]$. The theoretical r_0 computed from first principles approaches asymptotically the observed r_0 for large galaxies.

We see that the ratio M_{gal}/M_{virial} turns to be in the interval,

$$0.12 < \frac{M_{gal}}{M_{virial}} < 5.\ .$$

The contrast density, that is, the ratio between the maximum DM mass density $\rho_{lin}(0)$ and the average DM mass density $\bar{\rho}_{DM}$ in the universe results

$$\text{contrast} \equiv \frac{\rho_{lin}(0)}{\bar{\rho}_{DM}}$$

with $\bar{\rho}_{DM} = \Omega_{DM}\ \rho_c$ and Ω_{DM} and ρ_c given by eq.(15). $\rho_{lin}(0)$ is given by eq.(28) as

$$\rho_{lin}(0) = \frac{\mu_{0\,lin}}{r_0}\ .$$

We plot in fig. 9 the contrast density

$$\text{contrast} = \frac{\mu_{0\,lin}}{\Omega_{DM}\ \rho_c\ r_0} \tag{46}$$

As seen from fig. 9, the ratio obtained is between 1/3 and 1/2 of the observed value $\sim 3 \times 10^5$ in [40]. The values obtained are below the observed values because the linear halo radius $r_0 = r_{lin}/0.688$ is larger than the observed halo radius r_0 and the density contrast goes as $1/r_0$ eq.(46). This property shows again that the larger and more dilute is the galaxy the better is the linear approximation for non-universal quantities (see Table 2).

Notice that we consider the whole range of galaxy virial masses going from 5 to 300 $\times 10^{11}\ M_\odot$. Universal quantities as

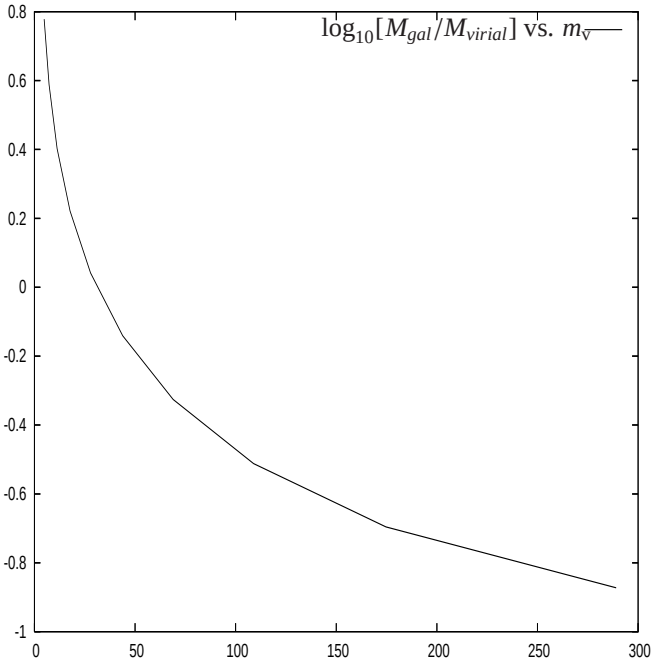

Figure 8: The common logarithm of the predicted total mass of the galaxy M_{gal} given by eq.(45), divided by the observed virial mass M_{virial} vs. the observed virial mass of the galaxy $m_v \equiv M_{virial}/[10^{11} M_\odot]$. The ratio M_{gal}/M_{virial} turns to be in the interval $0.12 < M_{gal}/M_{virial} < 5.0$. Notice that the difference of M_{gal} with M_{virial} is irrelevant to the determination of the DM particle mass.

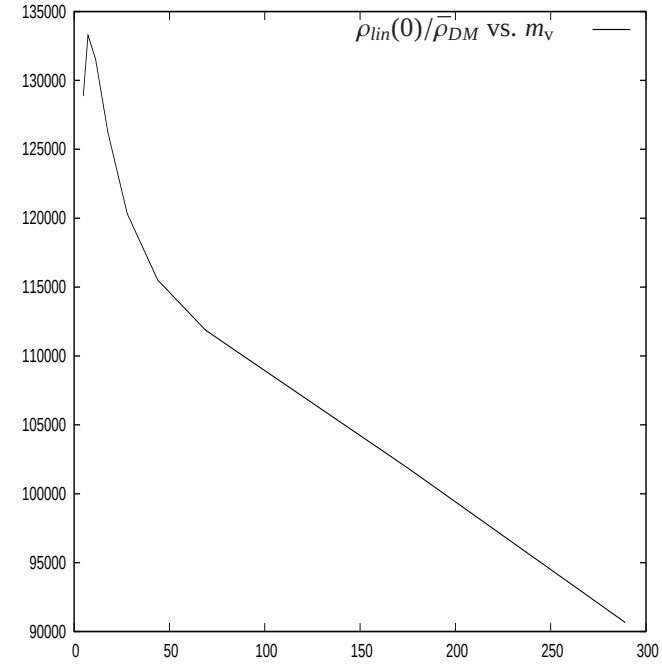

Figure 9: The ratio $\rho_{lin}(0)/\bar{\rho}_{DM}$ between the maximum DM mass density $\rho_{lin}(0)$ and the average mass density in the universe $\bar{\rho}_{DM}$ vs. the virial mass of the galaxy $m_v \equiv M_{virial}/[10^{11} M_\odot]$. The ratio $\rho_{lin}(0)/\bar{\rho}_{DM}$ turns to be between 1/3 and 1/2 of the observed value $\sim 3 \times 10^5$ [40].

the surface density stay constant up to ±20% within this wide range of galaxy masses.

It is relevant to evaluate the halo velocity given by eq.(A.4)

$$\overline{v^2}_{halo} = 2.316\, G\, \mu_0\, r_0\ . \tag{47}$$

Using eq.(44) this equation becomes

$$\overline{v^2}_{halo} = 6.705\, \frac{\mu_0}{\mathrm{MeV}^3}\, (\mathrm{km/sec})^2\, q_p^{-\frac{1}{3}}\ . \tag{48}$$

From Table 1 the input observed surface density takes the value

$$\mu_0 \simeq 6000\ \mathrm{MeV}^3\ . \tag{49}$$

Eq.(48) thus becomes

$$\sqrt{\overline{v^2}}_{halo\ lin} = \frac{201}{q_p^{\frac{1}{6}}}\ \mathrm{km/sec}\ . \tag{50}$$

The obtained range of values of q_p eq.(42) yields $q_p^{\frac{1}{6}} \simeq 0.77$ and

$$\sqrt{\overline{v^2}}_{halo\ lin} \simeq 260\ \mathrm{km/sec}\ . \tag{51}$$

This value is to be compared with the values arising from μ_0 and eq.(47) and the observed values r_0 in Table 1.

$$79.3\ \mathrm{km/sec} < \sqrt{\overline{v^2}}_{halo} < 261\ \mathrm{km/sec}\ . \tag{52}$$

The halo central density in the linear approximation is given from eqs. (44) and (49) by

$$\rho_{0\,lin} = \frac{\mu_0}{r_0} = 2.90\ 10^{-25}\, q_p^{\frac{1}{3}}\ \frac{\mathrm{g}}{\mathrm{cm}^3}\ .$$

Using the range of values of q_p eq.(42) obtained by solving eq.(36) yields

$$1.33\ 10^{-25}\ \frac{\mathrm{g}}{\mathrm{cm}^3} < \rho_0 < 1.94\ 10^{-25}\ \frac{\mathrm{g}}{\mathrm{cm}^3}\ ,$$

for 1.6 keV $< m <$ 1.9 keV, which must be compared with the observed values of ρ_0 given in Table 2.

We see that the linear approximation produces halo central densities smaller or in the range of the observations and halo velocities larger than the observed ones by a factor of order one.

Clusters of galaxies exhibit halo radius r_0 about 210 kpc [3] well beyond the linear halo radius $\sim$ 50 kpc. Hence, clusters of galaxies cannot be described by the initial conditions used here. Chosing general random fields $g(\vec{k}) \neq 1$ fulfilling eq.(26) will provide general configurations with a large range of masses and sizes. Each realization of the random field $g(\vec{k})$ produces a possible galaxy configuration. The factor $g(\vec{k})$ multiplies the transfer function $T(k)$ and therefore is to be added in the r. h. s. of eqs.(17), (23) and (32) and inside the $\vec{k}$–integrands [r. h. s. of eqs.(22), (27), (29), (30), (33), (34) and (35)].

We plot the density profiles in figs. 10 and 11. Fig. 11 displays 500 profiles averaged in the angles for random initial conditions. One can see that the random initial fluctuations only produce mild changes in the shape of the density profiles. Therefore, restricting ourselves for simplicity to initial primordial conditions with $g(\vec{k}) \equiv 1$ still provides relevant physical results.

	Observed Values	Linear Theory	Wimps in linear theory
r_0	5 to 52 kpc	46 to 59 kpc	0.0045 pc
ρ_0	1.57 to $19.3\times10^{-25}\ \frac{\text{g}}{\text{cm}^3}$	1.33 to $1.94\times10^{-25}\ \frac{\text{g}}{\text{cm}^3}$	$1.773\times10^{-14}\ \frac{\text{g}}{\text{cm}^3}$
$\sqrt{v^2}_{halo}$	79.3 to 261 km/sec	260 km/sec	0.0768 km/sec

Table 2: Non-universal galaxy quantities from the observations (Table 1 combined with the virial) and from the linear theory results. The corresponding dark matter particle mass is plotted in fig. 6 and is in the range 1.6 – 1.9 keV. The larger and less denser are the galaxies, the better are the results from the linear theory for non-universal quantities. The last column corresponds to 100 GeV mass wimps. The wimps values strongly disagree by several orders of magnitude with the observations.

7. The density profile: cores vs. cusps

The properties of the density profile $\rho_{lin}(r)$ depend on the free streaming length r_{lin} and therefore on the mass of the DM particle as we discuss here below.

We find from eqs.(28), (30) and (35) for the density profile at the origin

$$\rho_{lin}(0)=\frac{\mu_0}{r_0}=336.7\ b_1\ q_p^{\frac{n_s+2}{6}}\times\Big[1+0.04891\ \ln q_p\Big]\ \frac{(\text{MeV})^3}{\text{kpc}}\ . \quad (53)$$

We use from eqs.(39) and (44) that

$$q_p=\left(\frac{m}{m_0}\right)^4\quad,\quad r_{lin}=77.23\ \text{kpc}\ \left(\frac{\text{keV}}{m}\right)^{\frac{4}{3}}\ , \quad (54)$$

for DM particles decoupling ultrarelativistically at thermal equilibrium with m_0 given by eq.(40). Then eq.(53) can be written as

$$\rho_{lin}(0)=1.622\ 10^{-25}\ \left(\frac{m}{1.75\ \text{keV}}\right)^{1.976}$$
$$\times\left[1+0.2428\ \ln\left(\frac{m}{1.75\ \text{keV}}\right)\right]\ \frac{\text{g}}{\text{cm}^3}\ , \quad (55)$$

where we used the numerical values from eqs. (24) and (40) and the conversion of units:

$$\frac{(\text{MeV})^3}{\text{kpc}}=0.1483698\ 10^{-26}\ \frac{\text{g}}{\text{cm}^3}\ .$$

For the DM particle mass value $m\sim2$ keV found in the previous section, $\rho_{lin}(0)$ from eq.(55) is two to three times smaller than the observed values (as it is the contrast density, discussed in the previous section). This is not surprising because $\rho_{lin}(0)$ is not an universal quantity and given the approximation of our theoretical computation.

We derive in Appendix C, eq.(C.9) the density profile behaviour for $r\gtrsim r_{lin}$ where r_{lin} is given by eq.(54):

$$\rho_{lin}(r\gtrsim r_{lin})=10^{-26}\ \frac{\text{g}}{\text{cm}^3}\ \left(\frac{36.45\ \text{kpc}}{r}\right)^{1.482}$$
$$\times\ln\left(\frac{7.932\ \text{Mpc}}{r}\right)\ \left[1+0.2417\ \ln\left(\frac{m}{\text{keV}}\right)\right]\ . \quad (56)$$

It should be noticed that this behaviour has only a mild logarithmmic dependence on the DM particle mass m. The scales in eq.(56) only depend on known cosmological parameters and not on m.

We plot in fig. 10 the density profile $\rho_{lin}(r)$ according to eqs.(22) and (27) for DM particle masses m of 1 and 2 keV and the Burkert density profile for the largest galaxy $r_0=51.8$ kpc and $\rho(0)=1.57\times10^{-25}\ \frac{\text{g}}{\text{cm}^3}$ in Table 1. We see from fig. 10 that the density profile $\rho_{lin}(r)$ best follows the Burkert profile for a DM particle mass m slightly below 2 keV. This is in agreement with Fig. 6 for the DM particle mass where a value for m slightly below 2 keV is favoured.

We present in this paper clear evidences for a DM particle mass in the keV scale. However, one can wonder what is the shape of the density profile and the value of the density at the origin for a typical hundred GeV wimp.

Since wimps are supposed to decouple non-relativistically, eq.(11) does not apply to them. For DM particles decoupling non-relativistically Q_p is given by [12]

$$Q_p=\frac{\Omega_{DM}\ \rho_c}{2\ T_\gamma^3}\ g_d\ (m\ T_d)^{\frac{3}{2}}\quad\text{nonrelativistic decoupling}\ . \quad (57)$$

For a 100 GeV wimp decoupling at the typical temperature $T_{d\,wimp}=5$ GeV, we find from eqs.(31) and (57)

$$q_{p\,wimp}=0.3166\ 10^{21} \quad (58)$$

where we used that $g_d\simeq80$ at such decoupling temperature [30]. We then find from eq.(53) the central density value $\rho_{lin}(0)$ for such value of q_p:

$$\rho_{lin}(0)_{wimp}\simeq1.773\times10^{-14}\ \frac{\text{g}}{\text{cm}^3} \quad (59)$$

This value for the wimps density profile at the origin turns to be larger than the observed values by **eleven orders of magnitude**. This result indicates that the DM particle mass is not in the GeV scale. DM particles at the keV scale reproduce very well both the surface density and the density profile at the origin.

The free-streaming length r_{lin} is the characteristic scale where $\rho_{lin}(r)$ varies (see fig. B.14). This length is of the order of hundred kpc for keV mass scale DM particles as shown by eq.(54). For a hundred GeV wimp decoupling at $T_{d\,wimp}=5$ GeV we find from eqs.(43) and (58)

$$r_{lin}(m_{wimp}=100\ \text{GeV},\ T_{d\,wimp}=5\ \text{GeV})=0.0031\ \text{pc}=639\ \text{AU}\ .$$

Therefore, with such small r_{lin} for wimps we can use for all relevant galactic scales the asymptotic behaviour of $\rho_{lin}(r)$ eq.(C.8) valid for $r\gg r_{lin}$. That is,

$$\rho_{lin}(r\gtrsim0.003\text{pc})_{wimp}=0.8064\ 10^{-14}\ \frac{\text{g}}{\text{cm}^3} \quad (61)$$

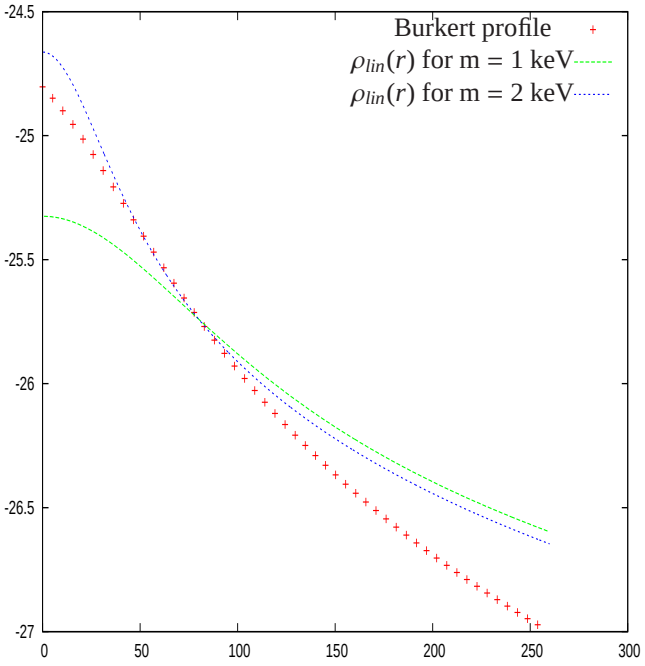

Figure 10: The common logarithm of the density profile $\rho_{lin}(r)$ according to eqs.(22) and (27) in g/cm^3 vs. r in kpc and the Burkert profile eq.(1). The Burkert profile is plotted with red crosses for the largest galaxy in Table 1 with $r_0 = 51.8$ kpc and $\rho(0) = 1.57 \times 10^{-25}\ \frac{\text{g}}{\text{cm}^3}$. Notice that the agreement of the linear density profile $\rho_{lin}(r)$ with the Burkert profile is best for a DM particle mass slightly below 2 keV.

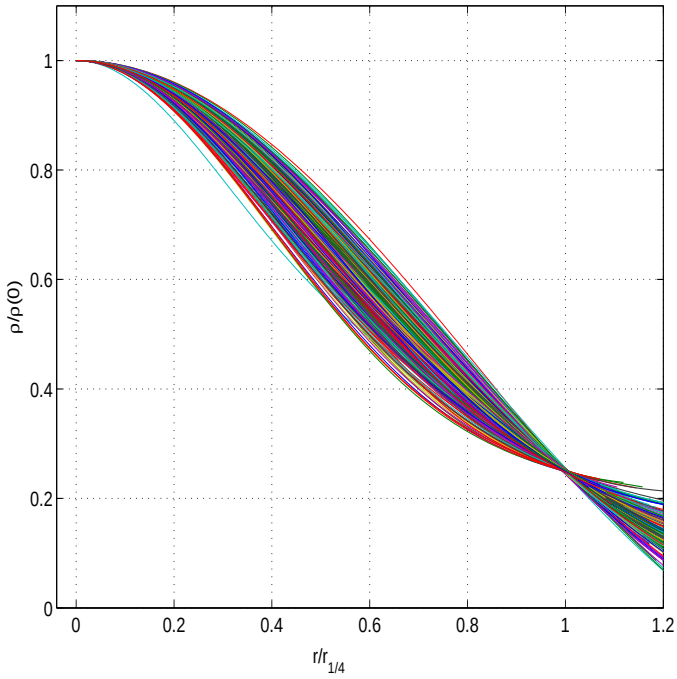

Figure 11: The normalized density profile $\rho_{lin}(r)/\rho_{lin}(0)$ averaged in the angles for 500 random initial conditions $g(\vec{k})$ vs. $r/r_{1/4}$ [11]. $r_{1/4}$ being the point where $\rho_{lin}(r)$ takes 1/4 of its value at the origin. $r_{1/4}$ coincides with the halo radius in the Burkert profile.

$$\times \left(\frac{0.0031\ \text{pc}}{r}\right)^{1.482} \left[1 + 0.04616\ \ln\left(\frac{0.0031\ \text{pc}}{r}\right)\right] .$$

This profile clearly exhibits a **cusp** behaviour for scales 1pc $\gtrsim$ r $\gtrsim$ 0.003 pc. Notice that this asymptotic formula eq.(61) approximatively matches around $r \sim 0.003$ pc the value of the wimp profile at the origin eq.(59).

In summary, the density profile $\rho_{lin}(r)$ eq.(22) exhibits a cusp around the origin for a wimp DM particle and a core behaviour at $r = 0$ for a keV scale DM particle mass.

We display in fig. 12 the density profile for 100 GeV wimps and the NFW profile for the largest galaxy in Table I. The density profile for 1-2 keV particles in fig. 10 and the density profile for wimps in fig. 12 practically coincide for $r \gtrsim 30$ kpc while they strongly differ at smaller scales ($r \lesssim 30$ kpc). The keV mass profile exhibits a core like the Burkert profile while the wimp profile exhibits a cusp like the NFW profile.

In this way, the value of the mass of the dark matter particle turns to be between 1 and 2 keV, and the number of ultrarelativistic degrees of freedom of the dark matter coupling at decoupling g_d, or similarly, the decoupling temperature T_d turns to be above 100 GeV.

We can also evaluate the halo velocity for wimps from the general formula eq.(50) and the value of $q_{p\ wimp}$ eq.(58). We obtain

$$\sqrt{\overline{v^2}}_{halo\ lin\ wimp} = 0.0768\ \text{km/sec}$$

three orders of magnitude below the observed halo velocities eq.(52). Recall that keV scale DM particles yield a halo velocity eq.(51) of the same order of magnitude than the observed halo velocities. Therefore, keV DM particles may solve the problem in the halo velocities recently noticed by [33] for the bullet cluster when CDM wimps are used.

The analytic expressions we derived for the density profile, and the mass of the dark matter particle also imply that keV dark matter particles always produce cored density profiles while heavy dark matter particles as wimps ($m = 100$ GeV, $T_d = 5$ GeV) inevitably produce cusped profiles at scales of 0.003 pc. These results are independent of the particle model and vary very little with the statistics of the dark matter particle.

8. On the Validity of the Linear Approximation

The linear approximation to the Boltzmann-Vlasov equation is valid as long as the density contrast is at most of order one. However, in the non-linear regime the density fluctuations relevant to the galaxy profiles grow with time independently of the wavenumber. Therefore, the shape of the linear profile survives in the non-linear regime. Only the profile normalization changes according with the non-linear evolution.

These results from linear approximation provide in principle only estimates since non-linear effects (including for instance mergers) are expected to be important. However, it turns out that the obtained linear results well reproduce the observations.

Of course, the theory of galaxy formation requires N-body simulations, beyond the scope of this paper.

Notice that general arguments based on the Boltzmann-Vlasov equation show that the cored or cusped character of a profile is preserved through mixing and mergers and that cusps do not become steeper neither shallower through mixing and mergers [10].

Therefore, the cored and cusped character we find for the linear profiles depending on the DM particle mass considered (keV and GeV mass scale, respectively) should remain valid after mixing and mergers are taken into account.

Moreover, recent N-body ΛCDM simulations (Acquarius) have found that the DM halos form in a sort of "monolithical" way [48]. Their inner regions, that contain the visible galaxies, are found to be stable since early times and contrary to previous believes, major mergers (i.e. those with progenitor mass ratios greater than 1:10) are found to contribute little to their total mass growth [48]. This indicates that nonlinearities (i.e. mergers) have a reduced importance. Minor mergers, secondary infall, rare major mergers are certainly important for details, but the essential features of DM halos are determined during the fast-accretion phase of their gravitational collapse, as the history of the quasar-galaxies coevolution also seems to indicate [25].

The halo formation essentially consists of two main phases: A first fast accretion phase (that can be treated by the linear approximation), and a second subsequent slow accretion phase with mergers and infalls, that have a random character and that can only be described by numerical simulations. This second phase does not have an essential influence in the shape of the halo profile. Thus, in order to explain the observed halo profiles one just needs to describe the first phase of halo formation, as we do here in this paper.

Evidence based on the phase space density pointing towards a DM particle mass in the keV scale was presented in refs. [5, 12]. Notice in this respect that the linear fluctuations as well as the spherical model (which contains the nonlinearities) both give values for the DM particle mass in the keV scale which only differ by a factor ten.

Analytic methods have been used to derive galaxy properties using the primordial power of the density fluctuations (see for example [26, 35]) and using the spherical model **(author?)** [1, 2].

In summary, the solution of the linearized Boltzmann-Vlasov equation presented here provides a satisfactory picture of the **general** galaxy properties. Although nonlinear effects and baryons are not taken into account, the linear description presented here qualitatively reproduces the main non-universal and general characteristics of a galaxy summarized in Table 2. Moreover, the agreement is even quantitative (approximatively) for the linear halo radius r_0, the galaxy mass M_{gal}, the linear halo central density ρ_0 and the halo velocity $\overline{v^2}_{halo\,lin}^{\,1/2}$ compared to the respectived observed values in the limiting case of large galaxies (both r_0 and M_{gal} large). The agreement is very good for universal galaxy quantities as the surface density and the density profile as discussed above.

The linear approximation for the density fluctuations amplitude today is clearly only an estimate for the true nonlinear value. However, the DM particle mass derived from the phase-space density in the linear approximation only differs by one order of magnitude from the nonlinear value obtained from the spherical model [12].

Interestingly enough, it is possible to derive the value of the surface density μ_0 from CDM simulations. Values of the product $r_s\ \rho_s$ from NFW fits to CDM simulations for galaxies were reported in [27]. From these values of $r_s\ \rho_s$ we can derive the surface density μ_0, since $\mu_0 = \rho_0\ r_0 \simeq 25\ r_s\ \rho_s$ with the result

$$\mu_0^{CDM} \simeq 10^7\ M_\odot/\mathrm{pc}^2\ . \qquad (62)$$

[Notice that ρ_s in [27] differs by a factor four from eq.(9)].

We see that the surface density from CDM simulations is **five orders** of magnitude **larger** than the observed surface density $\mu_{0\,obs} \simeq 120\ M_\odot/\mathrm{pc}^2$ [32, 17, 41].

It is illuminating to insert in eq.(36) the above value of the CDM surface density μ_0^{CDM} eq.(62)instead of the observed value $\mu_{0\,obs}$. This gives for the mass of the CDM particle $m^{CDM} \sim$ 60 GeV which is a typical wimp mass. Therefore, the linear approximation also provides a consistent value for the mass of the CDM particles in full agreement with CDM simulations.

These results show that our theoretical treatment captures many essential features of dark matter, allowing to determine its nature. When contrasted to the CDM surface density value obtained from CDM simulations (instead of the surface density value obtained from observations), our approach gives for the dark matter particle mass the typical CDM wimps mass scale (GeV), fully consistent with CDM simulations.

9. Conclusions

Dark matter is characterized by two basic quantities: the DM particle mass m and the number of ultrarelativistic degrees of freedom at decoupling g_d (or, alternatively the decoupling temperature T_d). We obtain the density profiles and theoretical relations between m and g_d involving the observable densities ρ_{DM} and μ_0 eqs.(11), (14) and (29). Inserting the observed values of ρ_{DM} and μ_0 in these theoretical relations yields m, g_d and Q_p eqs. (39)-(40) and (41), respectively.

We estimate the galaxy surface density and match it with the observed values. Within the same scheme, we derive analytically the halo radius r_0 and the factor Z characterizing the reduction of the phase-space density since equilibration till today. For these results we use the observed values of the halo phase-space density Q_{halo}.

From the observed values of the surface density we present here clear evidence that the mass of the DM particle is about one or two keV. Evidence based on the phase space density pointing towards a DM particle mass in the keV scale was presented in refs. [5, 12].

In addition, one can wonder what would be the results for heavy wimps. For example, for wimps at $m_{wimp} = 100$ GeV the

characteristic scale r_{lin} eq.(19) takes the value given by eq.(60). For such **small** r_{lin} the linear profile $\rho_{lin}(r)_{wimp}$ appears as a **cusped** profile when observed at scales from 0.003 pc to 1 pc as shown in fig. 12. Cusped profiles are thus clearly associated to heavy DM particles with a huge mass m_{wimp} well above the physical keV scale while cored profiles are associated to DM particles with mass in the keV scale.

Notice that the density profile turns out to be cored or cuspy depending on the DM particle mass m. For $m \sim$ keV the resulting density profile is cored as depicted in fig. 10 while for $m \gtrsim$ GeV the density profile turns to be cusped as shown in fig. 12. Figs. 10-12 show that the density profiles for a 1-2 keV DM particle are similar to Burkert (within a factor 2-3, irrelevant for the aims of this paper) while for a wimp DM particle, the density profile is similar to a NFW profile.

Despite its limitations, it is rather remarkable that the linear approximation is able to reproduce the observations within one order of magnitude. In the present paper we restrict ourselves to estimate the DM particle mass. In order to theoretically realize galaxy formation, N-body simulations must be performed with the appropriate primordial power spectrum. Such spectrum crucially depends for small scales on the value of the DM particle mass.

It must be stressed that the framework presented here applies to any kind of DM particles: particles with mass in the keV scale reproduce all observed galaxy magnitudes within one order of magnitude, while wimps ($m \sim 100$ GeV) present discrepancies with observations of up to eleven orders of magnitude. This is a robust indication that the DM particle mass is in the keV scale.

acknowledgments

P. S. thanks the Observatoire de Paris-LERMA and the LPTHE for the kind hospitality extended to him.

Appendix A. The average phase space-density

Q_{halo} in sec. 3 follows averaging $\rho(r)$ and $v^2_{halo}(r)$ over the volume. We define their average using the density $\rho(r)$ eq.(1) as weight function:

$$\overline{\rho} \equiv \frac{\int_0^{R_{vir}} r^2\, \rho^2(r)\, dr}{\int_0^{R_{vir}} r^2\, \rho(r)\, dr} \quad , \quad \overline{v^2}_{halo} \equiv \frac{\int_0^{R_{vir}} r^2\, \rho(r)\, v^2_{halo}(r)\, dr}{\int_0^{R_{vir}} r^2\, \rho(r)\, dr} \; . \tag{A.1}$$

The virial radius R_{vir} is defined by the radius where the mass computed from the Burkert profile eq.(1) takes the value [38]

$$M(R_{vir}) \simeq 10^{12}\, M_\odot \left(\frac{R_{vir}}{259\ \mathrm{kpc}}\right)^3 \; . \tag{A.2}$$

Here,

$$M(R_{vir}) = 4\,\pi \int_0^{R_{vir}} r^2\, \rho(r)\, dr = 2\,\pi\, \rho_0\, r_0^3$$

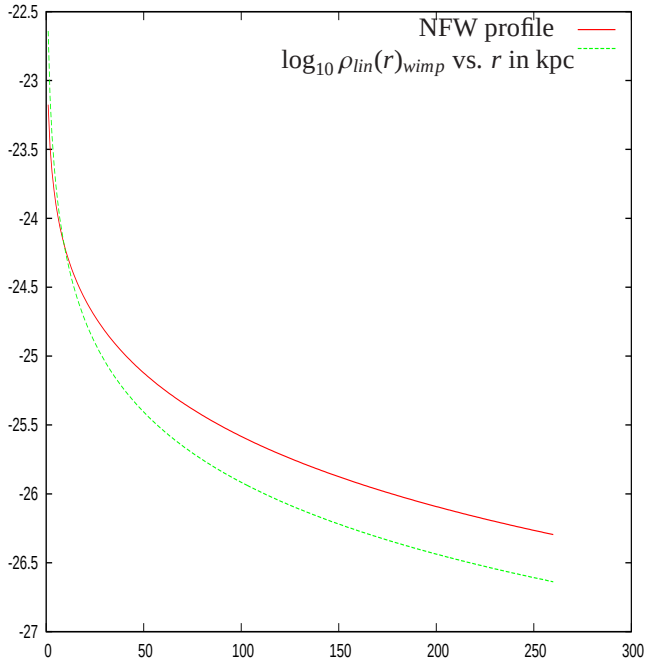

Figure 12: The linear density profile for 100 GeV wimps (broken green line) and the NFW profile (solid red line) for the same galaxy mass as the Burkert profile in fig. 10. In all cases the densities are in g/cm^3 and r in kpc. The wimps linear density profile follows eq.(C.8). The wimp linear profile exhibits a cusp like the NFW profile.

$$\times \left[\ln(1+\hat{c}) - \arctan\hat{c} + \frac{1}{2}\ \ln(1+\hat{c}^2)\right] \quad ,$$

$$\hat{c} \equiv \frac{R_{vir}}{r_0} \; . \tag{A.3}$$

Elliminating $M(R_{vir})$ between eqs.(A.2) and (A.3) gives $\hat{c}$ as a function of ρ_0 through the trascendental equation

$$\frac{\rho_0}{0.6187\ 10^{-27}\ \frac{\mathrm{g}}{\mathrm{cm}^3}} = \frac{\hat{c}^3}{\ln(1+\hat{c}) - \arctan\hat{c} + \frac{1}{2}\ \ln(1+\hat{c}^2)} \; .$$

The right hand side is a monotonically increasing function of $\hat{c}$. This implies that $\hat{c}$ increases when ρ_0 increases. Since r_0 decreases when ρ_0 increases (keeping constant the surface density μ_0), therefore $\hat{c}$ increases when r_0 decreases. For the galaxies in Table 1, we find $9.2 \lesssim \hat{c} \lesssim 24.9$, 120 kpc $< R_{vir} <$ 478 kpc, smaller values of $\hat{c}$ corresponding to larger galaxies.

From eqs.(4), (4) and (7) evaluating the integrals in eq.(A.1), we find

$$\overline{\rho} = 0.0662\, \rho_0 \quad , \quad \overline{v^2}_{halo} = 2.316\, G\, \rho_0\, r_0^2 \; , \quad ,$$

$$Q_{halo} = 3^{\frac{3}{2}}\, \frac{\overline{\rho}}{(\overline{v}^2_{halo})^{\frac{3}{2}}} = \frac{0.069}{G^{\frac{3}{2}}\ \sqrt{\rho_0}\ r_0^3} \; . \tag{A.4}$$

For the NFW profile eq.(9) the virial mass takes the form

$$M(R_{vir}) = 4\,\pi \int_0^{R_{vir}} r^2\, \rho(r)\, dr = 4\,\pi\, \rho_s\, r_s^3 \left[\ln(1+c) - \frac{c}{1+c}\right] \quad ,$$

$$c \equiv \frac{R_{vir}}{r_s} \ ,$$

and therefore we find for ρ_s,

$$\rho_s = 0.310\ 10^{-27}\ \frac{\mathrm{g}}{\mathrm{cm}^3}\ \frac{c^3}{\ln(1+c) - \dfrac{c}{1+c}} \quad . \tag{A.5}$$

The observations give for c the empirical relation [38]

$$c = 9.7\ \left(\frac{M(R_{vir})}{10^{12}\ M_\odot}\right)^{-0.13} \quad . \tag{A.6}$$

Therefore, knowing $M(R_{vir})$ and R_{vir} we obtain ρ_s and c from eqs.(A.5) and (A.6). For the galaxies in Table 1, we find 23.2 kpc $< r_s <$ 62.5 kpc , 0.439 10^{-25} g/cm^3 $< \rho_s <$ 1.087 10^{-25} g/cm^3 , 7.64 $< c <$ 13.1. We use the values of r_s and ρ_s for the larger galaxy to plot the NFW curve in fig. 12. Namely, r_s = 62.5 kpc and ρ_s = 1.087 10^{-25} g/cm^3.

Appendix B. The linearized density profile.

Both, the Burkert profile $F_B(r/r_0)$ eq.(1) and the linear profile $\Psi(r/r_{lin})$ eq.(27), have the same qualitative shape. To make the connection quantitative, we fit the linear profile with a Burkert profile setting

$$x = \alpha\ y \quad , \quad \text{that is,} \quad r_{lin} = \alpha\ r_0 \ . \tag{B.1}$$

We look for the value of α that gives the best fit by minimizing the sum of squares:

$$[\Psi(y) - F_B(\alpha\ y)]^2 \quad \text{for } 0 < y < 3 \ .$$

The best fit for each DM particle statistics is obtained for the values of α reported in Table B3. We display in fig. B.13 the Burkert profile $F_B(\alpha\ y)$ and the linear profiles $\Psi(y)$ for Fermi-Dirac, Bose-Einstein and Maxwell-Boltzmann statistics, respectively. We see from fig. B.13 that the profiles for Bose-Einstein and Fermi-Dirac statistics are better fitted by a Burkert profile than the profile for Maxwell-Boltzmann statistics.

We compute the behaviour of the linear profile $\rho_{lin}(r)$ eq.(22) for $r \gg r_{lin}$ in Appendix C. We find that the linear approximation can be used for (see Appendix C)

$$0 \le r < r_{max} \quad \text{where} \quad r_{max} \simeq 8 \text{ Mpc} \ .$$

It must be noticed that the maximum radius r_{max} turns to be independent of the DM mass m and only depends on known cosmological parameters.

We have at the origin $F'_B(0) = -1$ while $\Psi'(0) = 0$ and $\Psi''(0) < 0$. More precisely $\Psi''(0) = -2.74$ for fermionic DM particles. At the origin, the Burkert profile decreases with unit slope while the linear profile has an inverse-parabola shape.

Galaxy profiles take an universal form when $\rho(r)/\rho_0$ is expressed as a function of r/r_0. The Burkert profile is a particularly simple formula that satisfactorily reproduces the observations. The linear profile $\Psi(y)$, especially for Fermi-Dirac and Bose-Einstein statistics, fits very well the Burkert profile and therefore, $\Psi(y)$ is also able to well reproduce the observations.

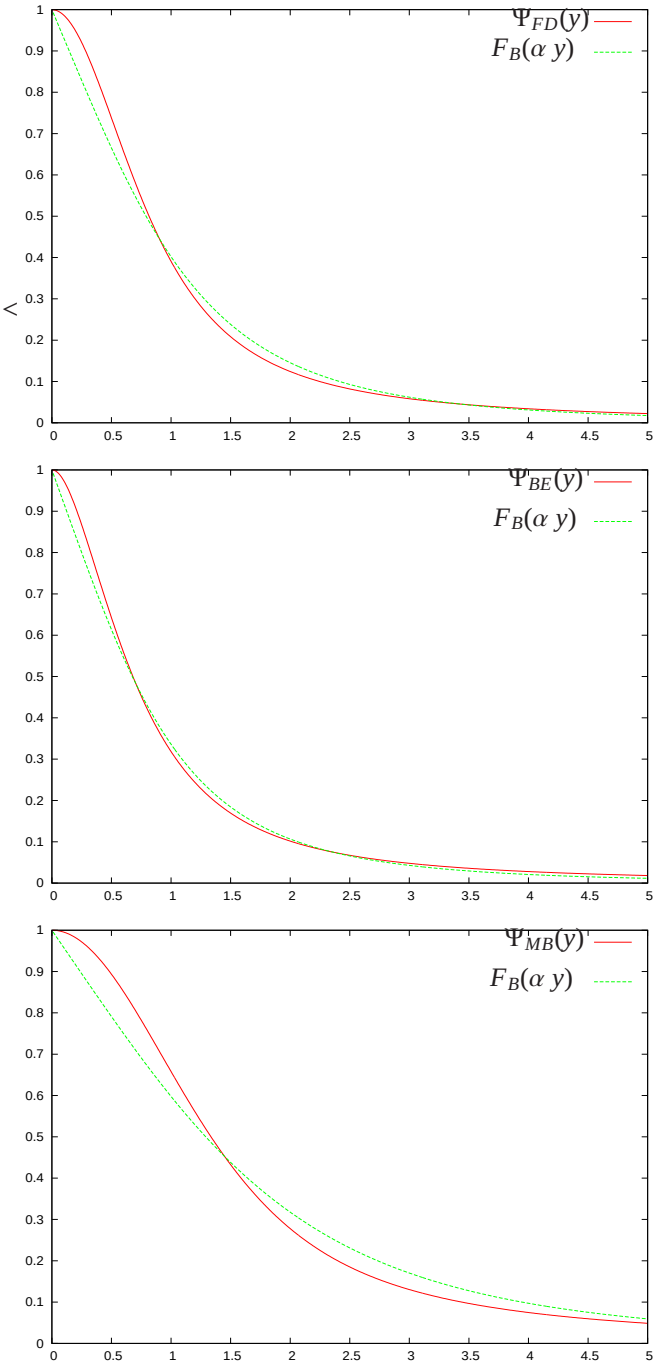

Figure B.13: The Burkert profile $F_B(\alpha\ y)$ and the linear profile $\Psi(y)$ computed from first principles vs. $y = r/r_{lin}$ for Fermi-Dirac (FD), Bose-Einstein (BE) and Maxwell-Boltzmann (MB) statistics. The values of α for each statistics are given in Table B3. The linear profile $\Psi(y)$, especially for Fermi-Dirac and Bose-Einstein statistics, fits very well the Burkert profile and as a consequence, $\Psi(y)$ reproduces the observations as well as $F_B(\alpha\ y)$.

Particle Statistics	α
Bose-Einstein	0.805
Fermi-Dirac	0.688
Maxwell-Boltzmann	0.421

Table B.3: The values of the parameter $\alpha \equiv r_{lin}/r_0$ for which the Burkert profile $F_B(\alpha\ y)$ best fits the linear profile $\Psi(y) \equiv \rho_{lin}(r)/\rho_{lin}(0)$, $y = r/r_{lin}$.

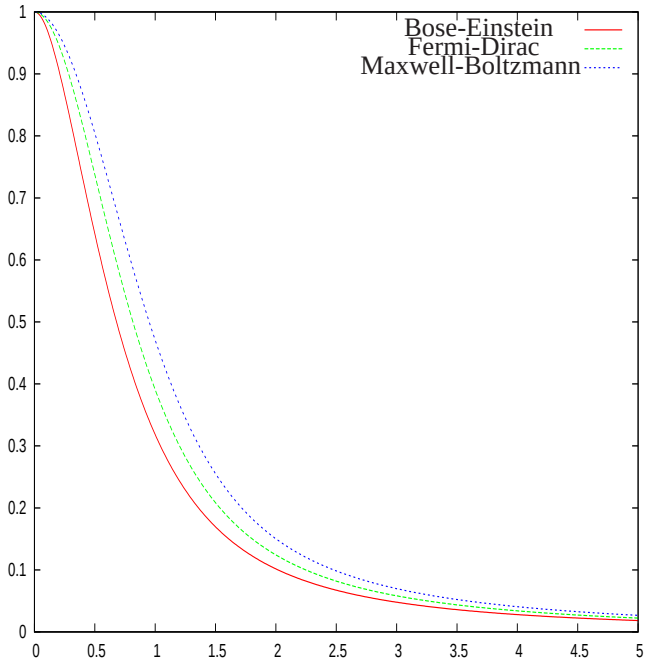

Figure B.14: The profiles $\rho_{lin}(r)/\rho_{lin}(0)$ vs. x, where $x \equiv r/r_{lin}$ for Fermions and Bosons decoupling ultrarelativistically and for particles decoupling non-relativistically (Maxwell-Boltzmann statistics). The bosons profile is the more peaked, the MB profile is the shallowest and the fermions profile is lying in-between. The profiles show little variation with the statistics of the DM particles.

Namely, the linear profile $\rho_{lin}(r)$ is well appropriated for small and intermediate scales

$$0 \leq r < r_{max} \ .$$

This means that although the linear approximation cannot capture the whole content of the structure formation, it can well reproduce **universal** features which are common to all types of galaxies as the density profile. Notice that the linear profile $\Psi(y)$ is universal as a function of $y = r/r_{lin}$. The values of r_{lin} and $\rho_{lin}(0)$ are not universal and change by orders of magnitude according to the halo mass. On the contrary, the surface density μ_0 defined by eq.(3) is an universal quantity. Indeed, the theoretical value of μ_0 that follows from the linear profile $\rho_{lin}(r)$ eq.(22) can reproduce the observed values of μ_0 as it has been shown in [13].

We use this property in section 4.1 to derive the values of the DM particle mass m and the number of ultrarelativistically degrees of freedom at decoupling g_d.

As shown above the linear profile and the Burkert profile are the closest for $r_{lin} = \alpha\ r_0$ with $\alpha = 0.688$. On the other hand, we know that the linear approximation always gives values for r_0 larger than the observed values, namely, the linear approximation improves for large galaxies [13]. Therefore, we require that r_{lin} tends to $r_0 \equiv 0.688\ r_0$ for large galaxies which fixes b_1 to be $b_1 \simeq 0.8$. In any case the dependence of the results on b_1 [which must be anyway $b_1 \sim 1$] is quite mild.

Appendix C. Asymptotic behaviour of the linear density profile.

To derive the asymptotic behaviour of $\rho_{lin}(r)$ it is convenient to change the integration variable in eq.(22) to

$$\eta \equiv \gamma\ \frac{r}{r_{lin}} \quad , \quad y = \frac{r}{r_{lin}} \ , \tag{C.1}$$

and we obtain

$$\Psi(y) = \frac{\rho_{lin}(r)}{\rho_{lin}(0)} = \frac{1}{y^2 \int_0^\infty \gamma\ N(\gamma)\ d\gamma} \times \int_0^\infty N\left(\frac{\eta}{y}\right) \sin\eta\ d\eta \tag{C.2}$$

In the limit $y = r/r_{lin} \to \infty$ we have from eq.(32)

$$N\left(\frac{\eta}{y}\right) \stackrel{y\gg 1}{=} \left(\frac{\eta}{y}\right)^{\frac{n_s}{2}-1} \left[\ln\left(\frac{c_0}{y}\ q_p^{\frac{1}{3}}\right) + \ln\eta\right]$$

where we used that $T(0) = 1$.

Therefore eq.(C.2) gives

$$\Psi(y) \stackrel{y\gg 1}{=} \frac{\Gamma\left(\frac{n_s}{2}\right) \sin\left(\frac{\pi}{4}\ n_s\right)}{\int_0^\infty \gamma\ N(\gamma)\ d\gamma}\ y^{-1-\frac{n_s}{2}} \times \left[\ln\left(\frac{c_0}{y}\ q_p^{\frac{1}{3}}\right) + \psi\left(\frac{n_s}{2}\right) + \frac{\pi}{2}\ \cot\left(\frac{\pi}{4}\ n_s\right)\right] \ , \tag{C.3}$$

where we used the formulas [24]

$$\int_0^\infty \eta^{\frac{n_s}{2}-1}\ \sin\eta\ d\eta = \Gamma\left(\frac{n_s}{2}\right) \sin\left(\frac{\pi}{4}\ n_s\right) \ ,$$

$$\int_0^\infty \eta^{\frac{n_s}{2}-1}\ \sin\eta\ \ln\eta\ d\eta = \Gamma\left(\frac{n_s}{2}\right) \sin\left(\frac{\pi}{4}\ n_s\right) \times \left[\psi\left(\frac{n_s}{2}\right) + \frac{\pi}{2}\ \mathrm{cotg}\left(\frac{\pi}{4}\ n_s\right)\right] \ , \tag{C.4}$$

$\psi(x)$ stands for the digamma function.

The asymptotic behaviour eq.(C.3) is hence governed by the small k behaviour of the fluctuations $\Delta(k, z_{eq})$ by the end of the radiation dominated era [see eq.(17)].

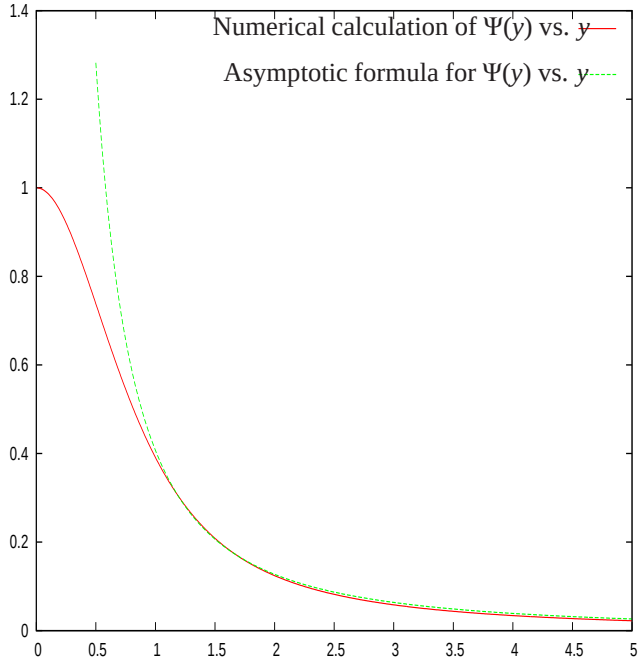

Figure C.15: The linear profile $\Psi(y)$ vs. y computed from the numerical Fourier transform eq.(27) in red continuous line and computed from the asymptotic formula eq.(C.5). We see that the asymptotic formula well reproduces the linear profile for $y \gtrsim 1$ and not just for $y \gg 1$.

Using the numerical values for n_s and c_0 from eqs.(24) and (32) and the integral over $N(\gamma)$ eq.(35), eq.(C.3) becomes

$$\Psi(y) \overset{y\gtrsim 1}{\simeq} \frac{0.4120}{y^{1.482}} \; \frac{1+0.1687\ln\left(\frac{q_p^{\frac{1}{3}}}{y}\right)}{1+0.04891\ \ln q} \; . \tag{C.5}$$

We obtain for DM particles decoupling ultrarelativistically at thermal equilibrium using eqs.(39) and (40),

$$\Psi(y) = 0.7705 \left(\frac{77.23\ \text{kpc}}{r}\right)^{1.482} \left(\frac{\text{keV}}{m}\right)^{1.976} \times \frac{1+0.1114\ln\left(\frac{\text{kpc}}{r}\right)}{1+0.2416\ \ln\left(\frac{m}{\text{keV}}\right)} \; , \tag{C.6}$$

where we used $1 + n_s/2 = 1.482,\ 2\,(2 + n_s)/3 = 1.976$.

We plot in fig. C.15 the asymptotic formula eq.(C.5) and the numerical Fourier transform eq.(27) for $\Psi(y)$. We see that the asymptotic formula eq.(C.5) correctly reproduces $\Psi(y)$ not only for $y \gg 1$ but for all $y \gtrsim 1$.

We see that there exists a maximum value y_{max} (and therefore r_{max}) where the linear profile vanishes:

$$y_{max} = 102.7 \left(\frac{m}{\text{keV}}\right)^{\frac{4}{3}} \quad , \quad r_{max} = 7.932\ \text{Mpc} \; . \tag{C.7}$$

where we used eqs.(C.1), (C.5) and (54).

Notice that r_{max} turns to be independent of the DM mass m and only depends on known cosmological parameters.

Thus, the linear approximation can be used for

$$0 \leq y < y_{max} \quad , \quad 0 \leq r < r_{max}$$

where $\Psi(y) > 0$ with y_{max} and r_{max} given by eq.(C.7).

The nonvalidity of the linear approximation beyond 8 Mpc reflects the fact that non-linear effects are important for small wavenumbers: this is consistent with the fact that we have effectively cutted off the modes $k < k_{eq}$ in the linear approximation [see eq.(25) and [13]] as it must be.

Combining the value of $\rho_{lin}(0)$ in eqs.(53) and (55) with the asymptotic behaviour eq.(C.5) yields

$$\rho_{lin}(r \gtrsim r_{lin}) = 10^{-26}\ \frac{\text{g}}{\text{cm}^3} \left(\frac{42.03\ \text{kpc}}{r}\right)^{1.482} \ln\left(\frac{7.932\ \text{Mpc}}{r}\right) \times \left[1 + 0.04891\ \ln q_p\right] \; . \tag{C.8}$$

We then find for DM particles decoupling ultrarelativistically at thermal equilibrium using eqs.(39) and (40),

$$\rho_{lin}(r \gtrsim r_{lin}) = 10^{-26}\ \frac{\text{g}}{\text{cm}^3} \left(\frac{36.45\ \text{kpc}}{r}\right)^{1.482} \ln\left(\frac{7.932\ \text{Mpc}}{r}\right) \times \left[1 + 0.2416\ \ln\left(\frac{m}{\text{keV}}\right)\right] \; , \tag{C.9}$$

where r_{lin} is given by eq.(54). It should be remarked that this behaviour has only a mild logarithmmic dependence on the DM particle mass m. The scales in eqs.(C.8)-(C.9) only depend on known cosmological parameters and not on m.

As noticed in **(author?)** [13], the asymptotic decrease of the linear profile given by eq.(C.8) is in remarquable agreement with the universal empirical behaviour put forward from observations in [47] and from ΛCDM simulations in [45]. For larger scales we would expect that the contribution from small k modes where nonlinear effects are dominant will give the customary r^{-3} tail exhibited by the Burkert profile eq. (1).

References

[1] E. Bertschinger, ApJS, 58, 1 (1985).
[2] E. Bertschinger, ApJS, 58, 39 (1985).
[3] A. Biviano, P. Salucci, Astronomy and Astrophysics, **452**, 75 (2006).
[4] G. Börner, *The Early Universe*, Springer, 2003.
[5] D. Boyanovsky, H J de Vega, N. G. Sanchez, Phys. Rev. **D 77**, 043518 (2008a).
[6] D. Boyanovsky, H J de Vega, N. G. Sanchez, Phys. Rev. **D 78**, 063546 (2008b).
[7] D. Boyanovsky, Phys. Rev. D78:103505, (2008).
[8] J. J. Dalcanton, C. J. Hogan, Astrophys. J. **561**, 35 (2001).
[9] W. J. G. de Blok, Advances in Astronomy, vol. 2010, pp. 1-15, arXiv:0910.3538.
[10] W. Dehnen, MNRAS 360, 892 (2005).
[11] C. Destri, private communication.
[12] H. J. de Vega, N. G. Sánchez, 2009a, arXiv:0901.0922, Mon. Not. R. Astron. Soc. 404, 885 (2010).
[13] H. J. de Vega, N. G. Sánchez, Int. J. Mod. Phys. A. 26, 1057 (2011).
[14] H. J. de Vega, N. G. Sánchez, arXiv:1111.0300, Phys. Rev. D, to appear.
[15] M J Disney et al. Nature 455, 1082 (2008), arXiv:0811.1554.
[16] Dodelson S, *Modern Cosmology*, Academic Press, 2003.
[17] F. Donato et al., MNRAS **397**, 1169 (2009).
[18] S. Ettori et al. arXiv:1009.3266, Astronomy and Astrophysics, in press.
[19] D. A. Garcia-Appadoo et al., Mon. Not. Roy. Astron. Soc. 394:340, (2009).

[20] G. Gentile et al., Nature, 461, 627 (2009).
[21] G. Gentile, C. Tonini, P. Salucci, A & A, 467, 925 (2007)
[22] I. H. Gilbert, Astrophys. J. **144**, 233 (1966); *ibid*, **152**, 1043 (1968).
[23] D. Gorbunov, A. Khmelnitsky, V. Rubakov JHEP 0812:055 (2008).
[24] I. S. Gradshteyn and I. M. Ryzhik, *Table of Integrals, Series and Products* Academic Press, N.Y. (1965).
[25] Granato G. L. et al. 2004, ApJ, 600, 580.
[26] Y. Hoffman and J. Shaham, Astrophysical Journal 297, 16 (1985).
[27] Y. Hoffman et al., Astrophysical Journal 671, 1108 (2007). We thank Yehuda Hoffman for communicating us that their units in fig. 4 are $M_\odot$ Mpc^{-2} and not $M_\odot$ kpc^{-2}.
[28] C. J. Hogan, J. J. Dalcanton, Phys. Rev. **D62**, 063511 (2000).
[29] W. Hu, N. Sugiyama, Astrophys. J. **471**, 542 (1996).
[30] E. W. Kolb, M. S. Turner, *The Early Universe*, Addison-Wesley (1990).
[31] E. Komatsu et al. (WMAP collaboration), Astrophys. J. Suppl. 180:330 (2009).
[32] J Kormendy, K C Freeman, IAU Symposium, Sydney, 220, 377 (2004), arXiv:astro-ph/0407321.
[33] J. Lee, E. Komatsu, arXiv:1003.0939, Astrophysical Journal 718 (2010) 60.
[34] K. Nakamura et al. (Particle Data Group), J. Phys. G 37, 075021 (2010)
[35] P J E Peebles, Astrophysical Journal 470, 16 (1984).
[36] K. Petraki, Phys. Rev. D77, 105004 (2008).
[37] M. Persic, P. Salucci, F. Stel, MNRAS, 281, 27 (1996).
[38] P. Salucci et al. MNRAS 378, 41 (2007)
[39] P. Salucci, Ch. Frigerio Martins, arXiv:0902.1703, EAS Publications Series, 36, 2009, 133-140.
[40] P. Salucci, M. Persic, ASP Proceedings 1997, astro-ph/9703027.
[41] M. Spano et al., MNRAS, 383, 297 (2008).
[42] F. D. Steffen, Eur. Phys. J. C59, 557 (2009).
[43] S. Tremaine, M. Henon, D. Lynden-Bell, Mon. Not. Roy. Astron. Soc. **219**, 285 (1986).
[44] S van den Bergh, arXiv:0810.3644, Nature 455, 1049 (2008).
[45] I. M. Vass et al., Mon. Not. R. Astron. Soc. **395**, 1225 (2009).
[46] M. Viel et al., Phys. Rev. D71, 063534 (2005).
[47] M. G. Walker et al., ApJ, 704, 1274 (2009).
[48] J. Wang et al.arXiv:1008.5114, MNRAS 413, 1373 (2011)..